

Assessment of the seismic capacity of mainshock-damaged reinforced concrete columns

A. Moshref^{1,2} · M. Khanmohammadi³ · M. Tehranizadeh⁴

Received: 12 April 2015 / Accepted: 28 May 2016 / Published online: 8 June 2016
© Springer Science+Business Media Dordrecht 2016

Abstract The objective of this study is to assess the post-earthquake capacity of reinforced concrete columns jointly using visual damage indicators and residual displacement. For this purpose, incremental dynamic analysis (IDA) is performed on the studied columns to correlate the maximum and residual drift ratios. Next, a method is developed to compute the fragilities of mainshock-damaged columns by performing IDA with a sequence of mainshock–aftershock ground motions. In this analysis, the mainshock is scaled to reach a particular damage state and after 5 s of rest time, aftershock ground motions are applied on the damaged columns. Then, the aftershock is scaled to result in collapse. Using the proposed methodology and the results of the IDA, fragility curves are developed for the damaged columns. Finally, modification factors are proposed to consider the effect of mainshock damage on the capacity curve of RC columns.

Keywords Modification factors · Aftershocks · Residual displacement · Fragility functions · Visual damage indicators

✉ A. Moshref
amir_moshref@yahoo.com; amir_moshref@aut.ac.ir

M. Khanmohammadi
mkhan@ut.ac.ir

M. Tehranizadeh
dtehz@yahoo.com

¹ Department of Civil Engineering, Islamic Azad University- Tafresh Branch, Tafresh, Iran

² Department of Civil and Environmental Engineering, Amirkabir University of Technology, Tehran, Iran

³ School of Civil Engineering, University College of Engineering, University of Tehran, Tehran, Iran

⁴ Department of Civil and Environmental Engineering, Amirkabir University of Technology, Hafez St., Tehran, Iran

1 Introduction

The past experiences from severe earthquakes around the world have shown that mainshock-damaged buildings are excited by a considerable number of aftershocks. Structures in Christchurch, New Zealand, experienced such a sequence of earthquakes when, first, a Mw 7.0 event in September 2010 and, subsequently, a Mw 6.1 event in February 2011 caused extensive damage to the built environment, much of which is still awaiting repair (Smyrou et al. 2011). The March 2011 Mw 9.0 earthquake in Tohoku, Japan, was followed by hundreds of aftershocks as large as Mw 7.9, including at least 30 aftershocks greater than Mw 6.0 (USGS 2011). In this situation, mainshock-damaged buildings are susceptible to excessive damage and even collapse caused by aftershocks, and thus, the loss of human life could be increased. Therefore, one of the preliminary proceedings after a major earthquake is to evaluate the performance of the damaged buildings. To this end, different assessment methods are proposed by guidelines and documents that can be grouped into two categories: (1) quick inspection methods and (2) detailed evaluation methods. One of the earliest published documents from the first group is ATC-20 (1989, 1995), which proposed procedures for post-earthquake rapid visual evaluation of buildings. The document contains guidelines for evaluating earthquake damaged buildings regarding the safety of their occupants.

The detailed evaluation methods analyze the future performance of the damaged structure by accounting for the effects of damage on the structural properties of the elements. For this purpose, the force–deformation behavior of damaged elements is estimated by modifying the behavior for their intact states and an analytical model of the damaged structure is built. The modification is determined based on the inelastic behavior mode (e.g., flexural, diagonal tension) and on the severity of the experienced damage. In 1999, ATC prepared the document FEMA-306: “Evaluation of Earthquake Damaged Concrete and Masonry Wall Buildings.” In this document, the severity of the damage is identified based on observable indications of damage, e.g., crack widths and concrete cover spalling. The effects of damage on wall behavior are modeled using three modification factors. The factors are used to modify the effective initial stiffness, the expected strength and the deformation acceptability limits based on the damage severity and the behavior mode. After the force–deformation behaviors of all structural components are predicted, the performance of the damaged structure is evaluated using pushover analysis. In Japan, the topic of evaluating damage to a structure and identifying technically and economically sound repair actions is addressed by JBDPA (2001). In this reference, an index based on the energy dissipation capacity of the damaged structural elements is employed to determine the seismic performance of damaged buildings. For this purpose, the maximum residual crack width is considered as a damage indicator.

Luco et al. (2004) proposed a probabilistic methodology to compute the residual capacity of mainshock-damaged buildings in terms of the ground motion intensity of an aftershock that can cause collapse or some other damage state. Using this methodology, Ryu et al. (2011) developed a methodology for developing fragilities for mainshock-damaged structures, “aftershock fragility,” by performing incremental dynamic analysis (IDA) with a sequence of mainshock–aftershock ground motions (back-to-back dynamic analysis). In their methodology, buildings are modeled using a damped single-degree-of-freedom (SDOF) nonlinear oscillator with force–deformation behavior represented by a multi-linear capacity/pushover curve with moderate pinching hysteresis and medium cyclic

deterioration. Ryu et al. defined median damage state threshold values in terms of the maximum roof displacement.

Visible damage indicators such as crack widths and concrete cover spalling are often subject to the engineer's judgment. In addition, the maximum roof displacement of a damaged structure is usually not available. Therefore, recent studies have been focused on more reliable parameters, such as residual displacement, which can be determined more reliably than other visual element indicators (Bazzurro et al. 2006; Yazgun 2009). The residual deformation as a result of component response inherently includes both the peak of displacement and the history of response (i.e., hysteretic behavior and cumulative energy dissipation capacity); hence, compared to other indicators, such as crack width and concrete cover spalling, this method is thought to be more reliable than other ones (Pampanin et al. 2003; Christopoulos et al. 2003).

However, post-earthquake observations after the September 2010 Christchurch earthquake show that many buildings with no residual displacements had to be repaired because of damage alone. Further evidence of damaged elements with no permanent displacement can be found in Shin's tests. Shin (2007) conducted shaking table tests on 12 single-story, single-bay reinforced concrete planar frames that consisted of two one-third scale columns connected by a rigid steel beam. Three types of experimental setups were used: Setup I specimens had two ductile columns, specimens with Setup II included one ductile column on the east side and one non-ductile column on the west, and specimens with Setup III consisted of two non-ductile columns. Four identical specimens were built for each experimental setup and subjected to a pulse-like ground motion with large velocity pulses (Kobe Earthquake) or long-duration motions with low velocity (Chile Earthquake). Two levels of axial loads were investigated in Shin's study, namely $0.1A_g f'_c$ and $0.24A_g f'_c$. The results showed that the ductile specimens with a high ratio of axial forces, $0.24A_g f'_c$, had almost no residual displacement, while their maximum drift ratios were equal to 5 and 6 %, respectively. Different levels of damage were also investigated. Thus, assessing the post-earthquake capacity of damaged elements or buildings using residual displacement alone as a damage indicator has a fundamental limitation, and the definition of damage states using joint damage indicators is inevitable.

The principle objective of this paper is to develop a methodology to quantify the post-earthquake capacity of reinforced concrete columns jointly using residual deformation and observable damage indicators. In this method, the probability of the collapse of a damaged column during aftershock is determined by performing IDA with a sequence of main-shock–aftershock ground motions. More specifically, two modification factors are proposed for the effective initial stiffness and the expected strength of damaged RC columns based on damage severity. By obtaining the modified force–deformation behaviors of damaged columns, the performance of the damaged structure can be evaluated using pushover analysis.

2 Experimental and modeling studies

2.1 Test specimens, test setup and procedures

A strong column database is available in the technical literature, but the definitions of different damage states are dependent on the observer and are therefore not uniform. Following this, this study considers five RC columns, which were tested by the third author

(Khanmohammadi 2006; Marefat et al. 2006). The main purpose of their study was to assess seismic vulnerability of existing low and mid-rise reinforced concrete buildings in Iran. To this end, cyclic and monotonic load tests on seven columns were carried out; four specimens represent existing buildings with deficient seismic details (special transverse reinforcements were not provided in the length of plastic hinges), and three others represent well-proportioned constructions in accordance with provisions of intermediate ductility, ACI318-99, which is a common reference in Iran. The dimensional scale of the specimens is 1:2, and the axial load has been proportioned to position on each column in the building. Five flexure-critical specimens among the aforementioned tests have been considered in this study. The details of the considered test specimens are shown in Fig. 1, and the amount of axial load and mechanical characteristics of the concrete and steel bars are listed in Table 1. The first letter in the sample names indicates whether it is designed based on ACI318-99 (S) or not (N). The second letter represents the location of the specimens in the height of the frame (T: top level and B: bottom level). The third letter shows the type of loading (C: cyclic loading and M: monotonic loading). The last letter represents the location of the specimens in the plan (M: interior and C: edge).

To obtain the mechanical properties of the reinforcing bars, tensile tests for steel coupons were conducted. Two coupons were tested for the specimen bars. Eighteen 6×12 in. standard cylinders were cast along with the columns and were used to measure the concrete compressive strength and stress–strain relationship. Compressive strength tests were performed at 8 and 29 days after casting the footing concrete and at 7, 14, 21, and 28 days after casting the column concrete. In each test, three cylinders were tested, and the mean 28-day concrete strengths of the columns are listed in Table 1.

The columns were tested in a vertical position, as shown on the loading setup in Fig. 2. Independent forces were applied simultaneously to the specimens using a 250-kN actuator for the axial load and one 100-kN actuator for the lateral loads. The axial load was applied in full magnitude at first and kept constant during the test as permanent load, and then the

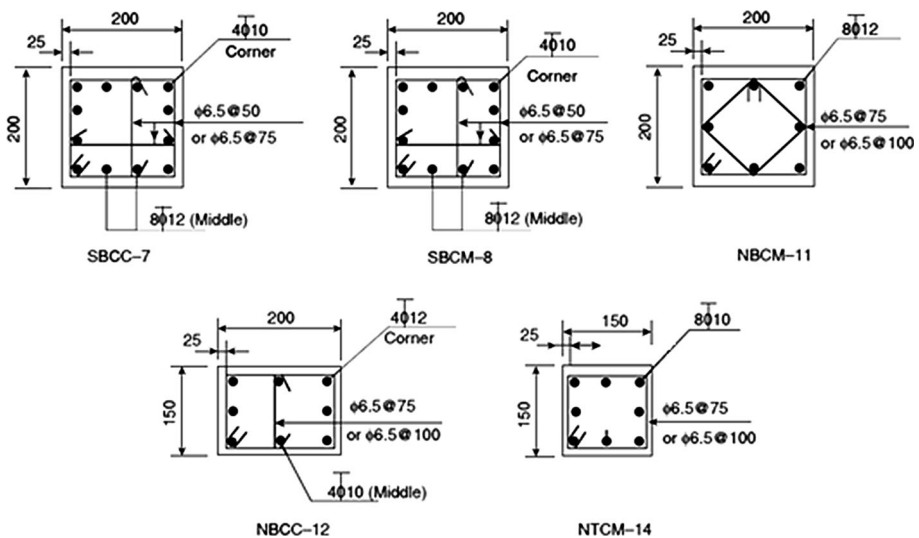


Fig. 1 The details of the test specimens (units in mm) (the term “or” in the figures indicates within or outside the plastic hinge region) (Khanmohammadi 2006; Marefat et al. 2006)

Table 1 The amount of axial load and mechanical characteristics of concrete and steel bars (Khanmohammadi 2006; Marefat et al. 2006)

Specimen	NTCM 14	NBCC 12	NBCM 11	SBCM 8	SBCC 7
Story	Top	Bottom	Bottom	Bottom	Bottom
Location in story	Middle	Corner	Middle	Middle	Comer
$P/A_g f'_c$	0.31	0.23	0.245	0.22	0.16
f'_c (MPa)	20.1	25.2	24.5	28	27
ρ_s (%)	2.8	2.5	2.26	3	3
ρ_v (%)	0.6	0.66	0.88	1.1	1.1
Longitudinal reinforcement					
Ultimate strain	0.18	0.18	0.18	0.18	0.18
Ultimate stress (MPa)	670	670	670	670	670
Elastic modulus (GPa)	204	203	203	203	203
Yield strain	0.002	0.002	0.002	0.002	0.002
Yield stress (MPa)	393	393	393	393	393
Stirrups					
Ultimate strain	0.25	0.25	0.25	0.25	0.25
Ultimate stress (MPa)	290	290	290	290	290
Yield strain	0.0012	0.0012	0.0012 </td <td>0.0012</td> <td>0.0012</td>	0.0012	0.0012
Yield stress (MPa)	220	220	220	220	220

f'_c = The mean 28-day concrete strength of the columns, ρ_s = longitudinal reinforcement ratio and is equal to the ratio of longitudinal reinforcement area to gross area of the column, ρ_v = lateral reinforcement ratio and is equal to A_s/Sd ; where A_s is lateral reinforcements area, S is spacing of stirrups, and d is effective depth

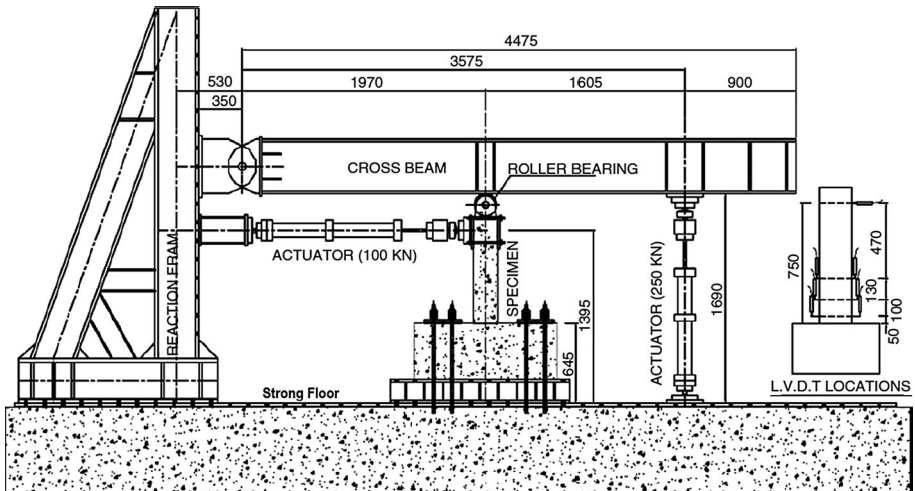
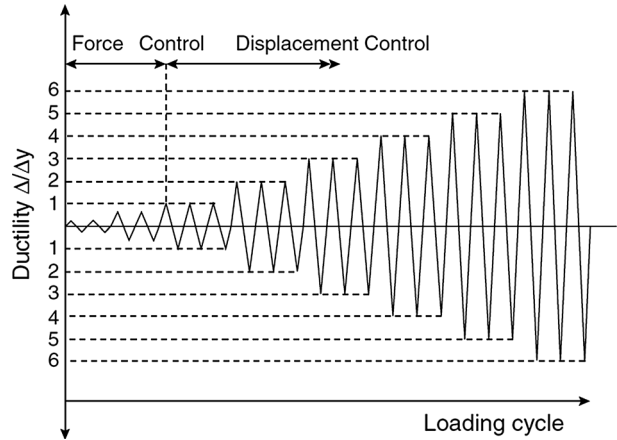


Fig. 2 Test setup and loading apparatus (units in mm) (Khanmohammadi 2006; Marefat et al. 2006)

lateral displacement history was applied cyclically. Laterally, the columns were subjected to single curvature bending where the loading path was controlled by lateral deformations, as shown in Fig. 3. LVDTs and strain gages were used to measure the lateral deflection, the

Fig. 3 Specified displacement history at the location of actuator (Khanmohammadi 2006; Marefat et al. 2006)



vertical deformation and the rotation, while electrical resistance gauges were used to measure the steel strains. A microcomputer and an automatic acquisition system were used to record the data.

2.2 Test results and observed behavior

All of the specimens developed their full flexural yield strength, and no shear failure was observed during the tests. As a general behavior, flexural cracks formed at the bottom of the column from the first lateral loading cycle, followed later by inclined cracks with each cycle. When the deflection increased, the inclined cracks propagated, their number increased and their widths widened. During the unloading stages, the formed cracks, depending on the level of lateral loading cycle, closed completely or partially, or narrowed to their minimum width.

Table 2 lists the drift ratios corresponding to different damage states for the studied specimens based on experimental data. The reported drift is the ratio of lateral displacement applied to horizontal actuator, installed on height of 1395 mm from strong floor, down to critical section on foundation. The column shear force–lateral displacement responses for all models are shown in Fig. 4.

2.3 Mathematical modeling of the studied columns

The authors (Moshref et al. 2014) investigated the reliability of different nonlinear modeling approaches to capture the residual displacement of RC columns. They found that

Table 2 Corresponding drift ratios (at the location of the actuator) at different damage states

Specimens	SBCC-7	SBCM-8	NBCM-11	NBCC-12	NTCM-14
First yield of reinforcement (%)	0.8	0.5	1.0	0.8	0.5
Concrete spalling drift (%)	2.0	1.6	1.6	2.4	1.9
Concrete crushing drift (%)	3.2	4.8	2.7	3.2	3.8
Bar buckling drift (%)	6.4	5.9	6.7	7.2	5.9

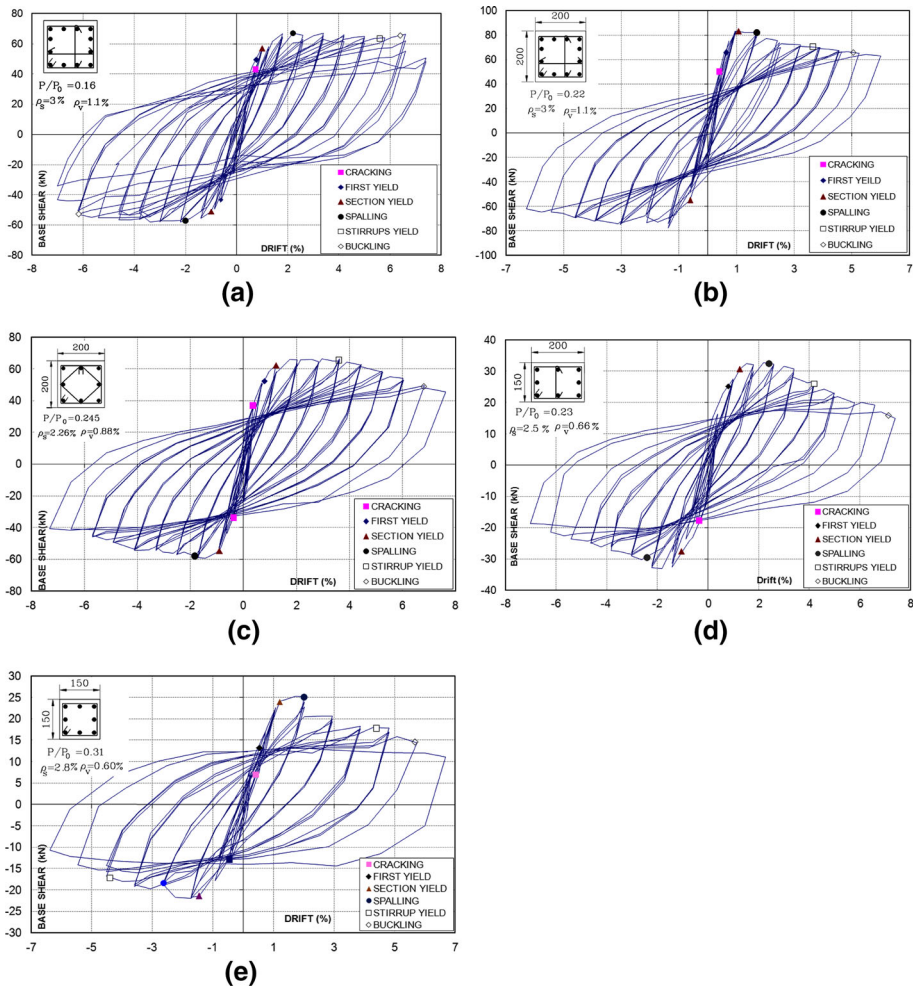


Fig. 4 Base shear-lateral displacement responses for all specimens (the effect of P-Δ on lateral force has been considered) (Khanmohammadi 2006; Marefat et al. 2006). *Notation* P = axial force (kN), P_0 = nominal strength of section under axial force (kN), ρ_s = longitudinal reinforcement ratio, ρ_v = lateral reinforcement ratio. **a** SBCC-7, **b** SBCM-8, **c** NBCM-11, **d** NBCC-12, **e** NTCM-14

steel and concrete constitute behaviors and that viscous damping modeling plays a crucial role in the capability of different modeling approaches to capture the residual displacement. Therefore, their recommended modeling approach was implemented in this study, as is illustrated in the following paragraphs.

The finite-element models of the studied specimens were built using OpenSees (2002), as shown in Fig. 5. A fiber section was constructed using reinforcing steel fibers and fibers with different properties for the unconfined and confined concrete. A total of 64 concrete fibers were used for modeling the RC section (36 for confined concrete fibers and 28 for unconfined concrete fibers) based on the parametric study using test data. The displacement-based beam column elements with five integration points were used to model the

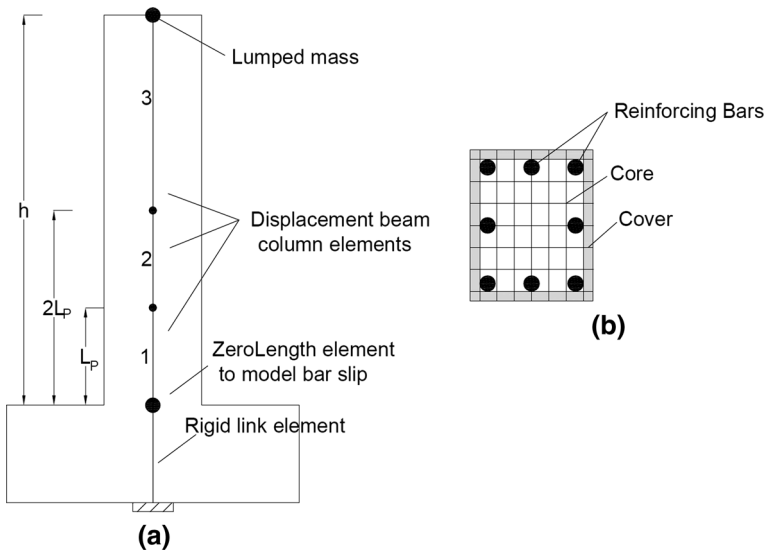


Fig. 5 a Distributed finite element model of the studied columns, b fiber section discretization

specimens. For all of the columns, the plastic hinge length was calculated with the Paulay and Priestley equation (1992) as below:

$$L_p = 0.08L + 0.022f_y d_b \tag{1}$$

where L is the distance of the critical plastic hinge section from the estimated point of contraflexure, f_y is probable yield strength of longitudinal reinforcement, and d_b is the nominal diameter of longitudinal reinforcement.

Although the above mentioned elements can accurately capture behaviors such as the initiation of concrete cracking and steel yielding, they can be limited in their ability to capture strength degradation, such as bond slip and shear failure. Therefore, the bar slip effect was modeled using elastic rotational springs, and their stiffness was calculated based on the equation from Elwood and Moehle (2003), as below:

$$K_{slip} = \frac{8u}{d_b f_s} EI_{flex} \tag{2}$$

where d_b is the nominal diameter of the longitudinal reinforcement, EI_{flex} is the effective flexural rigidity obtained from a moment–curvature analysis of the column section, u is the bond stress and is equal to $0.8\sqrt{f'_c}$ (in MPa units), f'_c is the concrete compressive strength, and the stress in the longitudinal reinforcement (f_s) can be taken as equal to the yield stress (f_y) for columns with low axial loads.

The ReinforcingSteel material model was used in OpenSees to model the longitudinal reinforcing steel in the specimens. The ReinforcingSteel model uses a nonlinear backbone curve shifted as described by Chang and Mander (1994) to account for isotropic hardening (Fig. 6a). To account for changes in the diameter of the bar during yielding, the backbone curve is transformed from engineering stress space to natural stress space. The softening region (strain greater than e_{ult}), shown in Fig. 6a, is a localization effect due to necking and is a function of the gauge length used during measurement. This geometric effect is

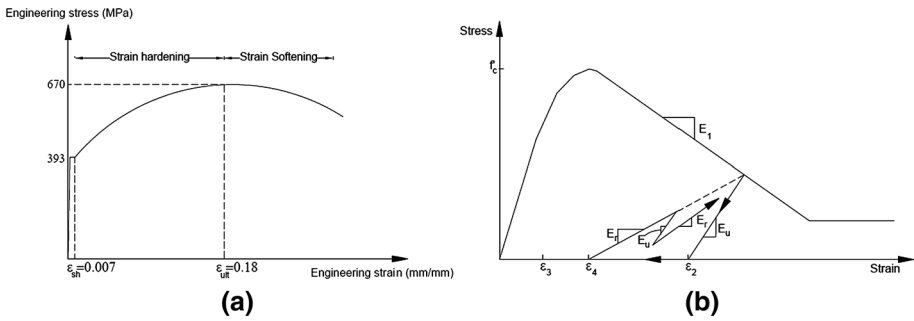


Fig. 6 **a** ReinforcingSteel material model, **b** concrete material model (Stanton and McNiven 1979)

ignored in this simulation. This simulation assumes that there is no softening in the natural stress space, allowing the single backbone to represent both the tensile and compressive stress–strain relations. The tension and compression backbone curves are thus not the same in the engineering stress space for this model. In this model, several buckling options can be used to simulate the buckling of the reinforcing bar, but these options are not used for the analysis in this research.

Lee and Billington (2010) found that using a conventional constitutive model for concrete behavior displays the pinched response in the fiber-element model, which eliminates residual displacement. Following this, they implemented a modified concrete constitutive model that incorporates changes in the reloading behavior when moving from high tensile strain to compression side during the reloading path. In the modified model, the concrete reloads in compression at a lower strain value than the previous unloading strain. The model is peak oriented, i.e., the stress path during reloading will aim toward the peak point (the maximum compressive strain reached) on the envelope curve. For simplicity, they assumed that the reloading strain (ϵ_r) is equal to a constant positive value. Because the reloading strain is set at a constant positive value, the model will function in exactly the same manner as the original concrete model if this value is not exceeded, i.e., if the concrete does not go too far into tension. The authors (Moshref et al. 2014) found that using constant positive reloading strain could not capture the permanent displacement well. Therefore, they considered unloading strain as a function of the proportion of crack filled by rubble based on the Stanton and McNiven model (1979), as below.

$$\epsilon_4 = \epsilon_2 - r(\epsilon_2 - \epsilon_3) \tag{3}$$

where r is the empirical constant. If $(\epsilon_2 - \epsilon_3)$ is greater than a limiting value CMX , then $(\epsilon_2 - \epsilon_3)$ is replaced by CMX (Stanton and McNiven 1979). Based on the calibration study carried out by the authors (Moshref et al. 2014), the values of r and CMX are considered equal to 0.2 and 0.03, respectively. Figure 6b illustrates the concrete material model that was used in this study.

P-delta effects were considered by transforming the element forces and deformations between local and global coordinate systems, using the geomTransf command in Opensees. The damping ratio was considered equal to 2 % for all specimens, and the stiffness-only proportional damping matrix was used in the analytical models. Figure 7 compares the experimental and numerical hysteretic behavior of the studied specimens. Figure 7 shows that the analytical strength/stiffness of some columns degraded faster than in the actual tests because of the modeling assumptions. The horizontal component of the vertical actuator is not considered in the mathematical model.

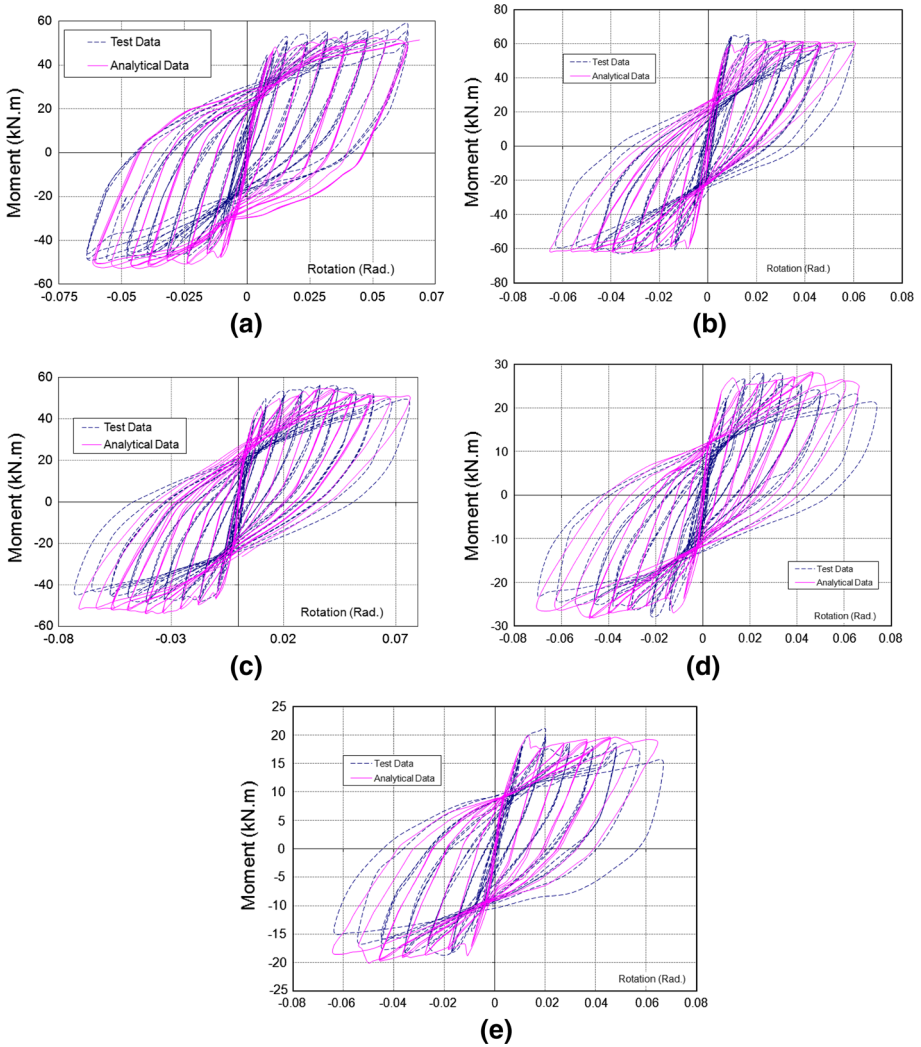


Fig. 7 Numerical and experimental hysteretic behavior of the studied specimens. **a** SBCC-7, **b** SBCM-8, **c** NBCM-11, **d** NBCC-12, **e** NTCM-14

3 Methodology to develop fragility surfaces

3.1 Fragility for intact columns

In this study, a collapse fragility function defines the probability that a column experiences bar buckling, as a function of ground motion intensity. The Fragility curves can be computed using the following Equation:

$$\begin{aligned}
 &P(DS \geq \text{Bar buckling} | IM = im) \\
 &= \int P(DS \geq \text{Bar buckling} | \Delta_{\max} = \delta) \times f(\Delta_{\max} = \delta | IM = im) d\delta
 \end{aligned}
 \tag{4}$$

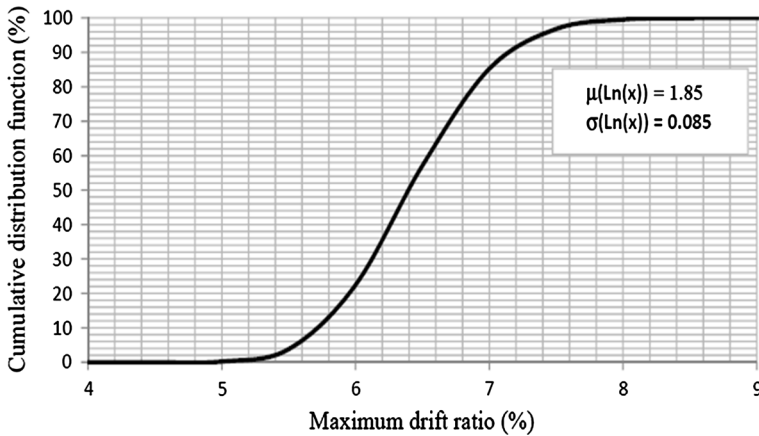


Fig. 8 Cumulative distribution function (CDF) of the maximum drift ratio corresponding to bar buckling

where DS denotes the damage state, IM denotes the ground motion intensity (e.g., spectral acceleration), and Δ_{max} denotes the maximum drift ratio. The first term in Eq. (4), $P(DS \geq \text{Bar buckling} | \Delta_{max} = \delta)$, represents the probability of being in or exceeding the bar buckling given δ and can be computed as:

$$P(DS \geq \text{Bar buckling} | \Delta_{max} = \delta) = P(\Delta_{max, \text{Bar buckling}} \leq \delta) \tag{5}$$

where $\Delta_{max, \text{bar buckling}}$ represents the maximum drift ratio corresponding to bar buckling. To calculate Eq. (5), the maximum drift ratios corresponding to bar buckling are assumed to be log-normally distributed random variables and the distribution parameters are estimated using the maximum likelihood method and the data of Table 2, as shown in Fig. 8.

The second term, $f(\Delta_{max} = \delta | IM = im)$, represents the probability distribution of the maximum drift ratio on the column for a specified ground motion intensity level and was computed using the results of the IDA of the specimens under 22 far field ground motion records, as presented in Sect. 4.1.

3.2 Fragility surfaces for mainshock-damaged columns

As presented in the Sect. 1 above, it is possible to have severe damage in buildings without any significant residual displacement. Following this, both permanent displacement and visual damage indicators are considered here to develop the fragility curves for mainshock-damage columns. In accordance with the total probability theorem, the fragility function can be computed using Eq. (6). To derive this equation, the permanent displacement is considered conditionally independent of visual damage indicators given maximum drift ratio.

$$\begin{aligned} &P(DS_a \geq \text{Bar buckling} | IM_a = im_a, DS_m = ds_m, \Delta_{residual, m} = \delta_{r, m}) \\ &= \int \int P(DS_a \geq \text{Bar buckling} | \Delta_{max, a} = \delta_a) \\ &\quad \times f(\Delta_{max, a} = \delta_a | IM_a = im_a, \Delta_{max, m} = \delta_m) \\ &\quad \times \frac{f(\Delta_{max, m} = \delta_m | DS_m = ds_m)}{P(\Delta_{max, m} = \delta_m)} \\ &\quad \times f(\Delta_{max, m} = \delta_m | \Delta_{residual, m} = \delta_{r, m}) d\delta_m d\delta_a \end{aligned} \tag{6}$$

where DS_a represents the post-aftershock damage state, DS_m represents the post-main-shock damage state, $\Delta_{max,m}$ and $\Delta_{max,a}$ represent the maximum drift ratio of the column during mainshock and aftershock, respectively, $\Delta_{residual,m}$ represents the residual drift ratio after a mainshock, and IM_a represents the ground motion intensity of an aftershock. Figure 9 illustrates the methodology to calculate the fragility function based on Eq. 6. The different terms of this method can be calculated as below:

The probability $f(\Delta_{max,m} = \delta_m | DS_m = ds_m)$ of δ_m conditioned on the detection of the visual damage indicator ds_m can be computed using Bayes' Theorem, as below:

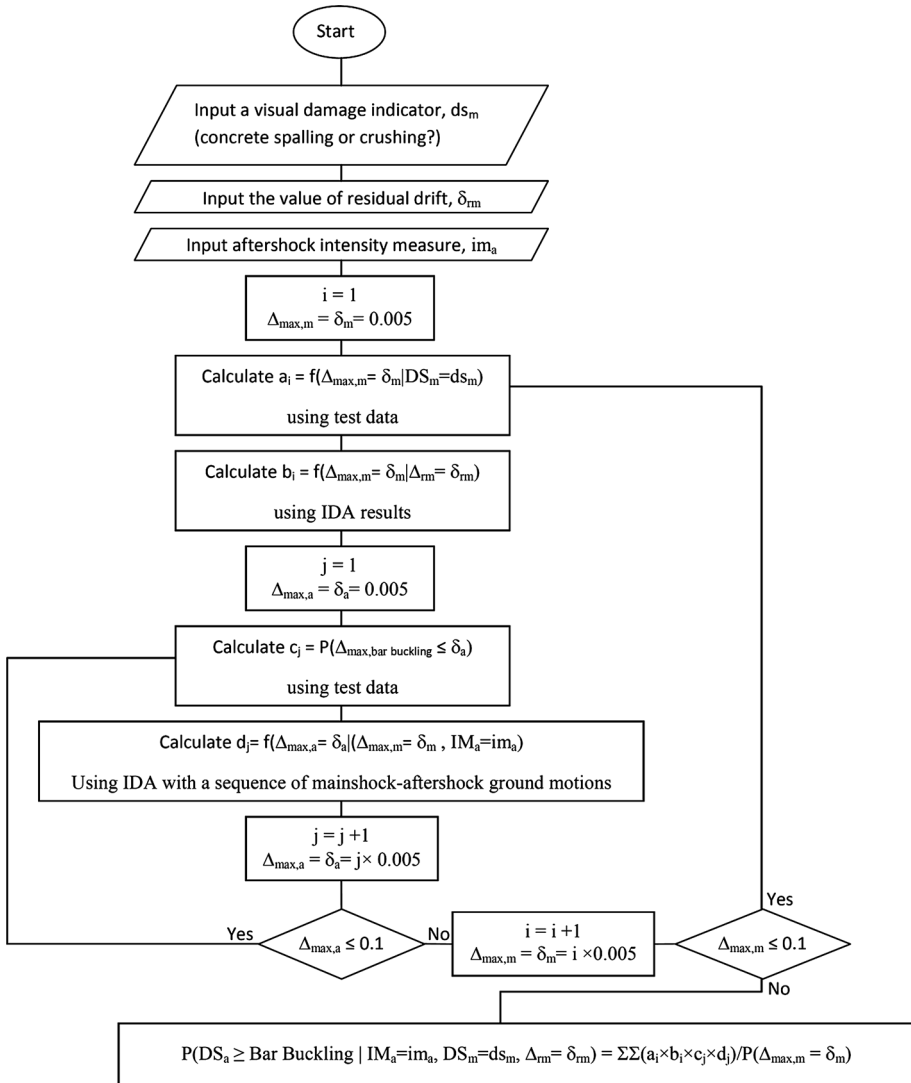


Fig. 9 Methodology to calculate the fragility function of mainshock-damaged columns

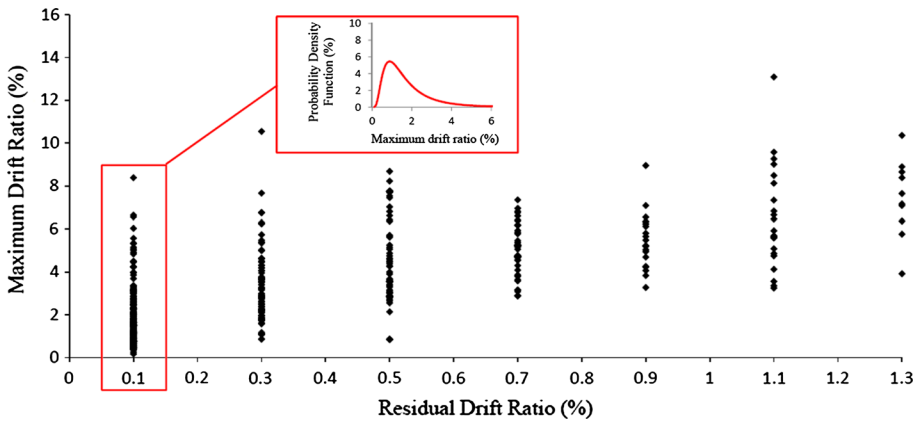


Fig. 10 Maximum drift ratio versus residual drift ratio

$$f(\Delta_{max,m} = \delta_m | DS_m = ds_m) = \frac{f(DS_m = ds_m | \Delta_{max,m} = \delta_m) \Pr(\Delta_{max,m} = \delta_m)}{\sum_{i=1}^{20} f(DS_m = ds_m | \Delta_{max,m} = \delta_i) \Pr(\Delta_{max,m} = \delta_i)} \quad (7)$$

where $f(DS_m = ds_m | \Delta_{max,m} = \delta_i)$ can be computed using the described method for Eq. 5.

The probability of the maximum drift ratio, $\Delta_{max,m}$, conditional on the measured residual drift ratio, $\Delta_{residual,m}$, can be computed by performing IDA on the intact columns. To this end, the maximum and residual drift ratios should be captured for each record in each intensity level. Figure 10 shows a graph of the maximum drift ratio, $\Delta_{max,m}$, versus the residual drift ratio, $\Delta_{residual,m}$, using the results of the IDA of the five studied specimens under 22 ground motion records, as presented in Sect. 4.1. In this graph, the numbers on the residual drift ratio axis are divided into ranges of 0.2 %, and the median interval was used to show the data. In next step, the probability density functions of each series can be found using the P value and maximum likelihood method. The probability density function of the maximum drift ratio corresponding to the values of the residual drift ratio in the range between 0 and 0.002 is shown in Fig. 10.

The probability $f(\Delta_{max,a} = \delta_a | IM_a = im_a, \Delta_{max,m} = \delta_m)$ can be computed by performing IDA with a sequence of mainshock–aftershock ground motions. In this analysis, the columns are subjected to a mainshock–aftershock sequence, as shown in Fig. 11. The mainshock record is scaled to reach maximum displacement equal to δ_m , and then an aftershock record is applied to the mainshock-damaged column. A rest time of 5 s is added between consecutive earthquake events. A total of 484 earthquake sequences were created by combining each of the 22 mainshock ground motions, which are presented in Sect. 4.1, with the same 22 ground motions applied as aftershocks. In the last step, the probability of the bar buckling (collapsed) conditional on the maximum drift ratio during aftershock, $P(DS_a \geq \text{Bar buckling} | \Delta_{max,a} = \delta_a)$, can be computed using Eq. 5.

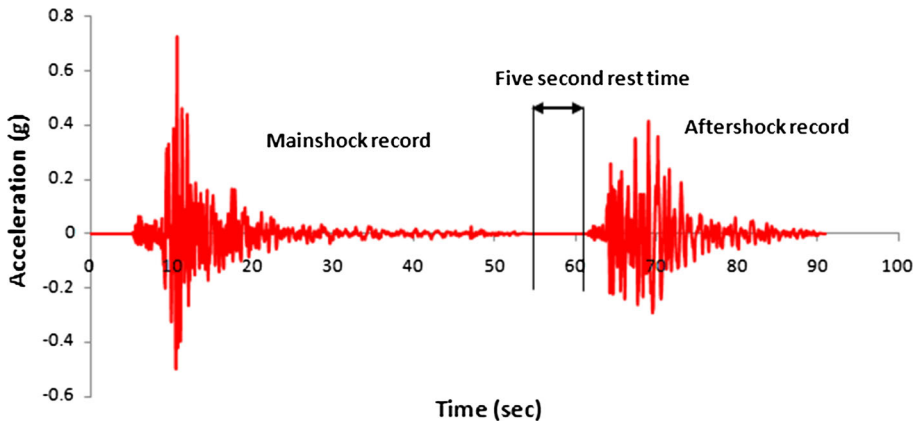


Fig. 11 A mainshock–aftershock sequence

4 Nonlinear dynamic analysis

4.1 Mass definition

To define a reference frame, more than 70 buildings in Tehran have been inspected by the third author (Khanmohammadi 2006). The inspection comprises reviews of structural drawings, site inspection, and reference to active workshops. The survey indicates significant similarities among this type of building, including:

- The structural frames have span lengths between 5 and 5.5 m in both directions.
- The height of the first story is 3.0 m and that of other stories is 3.2 m.
- The number of columns per 1 m² of built area varies between 0.08 and 0.10.
- The dimensions of the beam and column sections of different buildings are close to each other.

The reference frame has been designed according to ACI318-99, the seismic provisions of intermediate ductility, which is commonly used in Iran. The frame model geometry, along with the beam and column sections and the reinforcement properties, is shown in Fig. 12. The hysteretic behavior of the elements of the reference frame was studied by the third author using cyclic tests. It should be noted that the specimens presented in the “Test specimens, test setup and procedures” section above have been a part of his study to investigate the behavior of the columns of the aforementioned frame. Figure 13 shows the capacity/pushover curve of the reference frame using a 1st mode shape load pattern.

The columns examined in this study aim to be representative of those found in the reference frames; hence, the lumped mass of the specimens is calculated as below.

The capacity base shear of the elasto-plastic equivalent single-degree-of-freedom system (V_y^*) with similar period and yielding displacement (u_y) to the multiple-degree-of-freedom (MDOF) model can be calculated using the following equation (Clough and Penzien 1993):

$$V_y^* = k^* u_y = m^* \omega^2 u_y \quad (8)$$

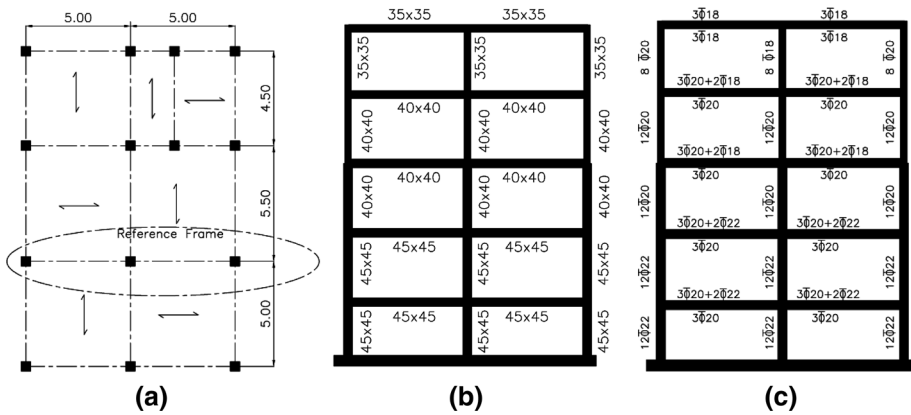


Fig. 12 **a** Column layout (units in m), **b** beam and column section (units in cm), **c** reinforcement properties of the reference frame

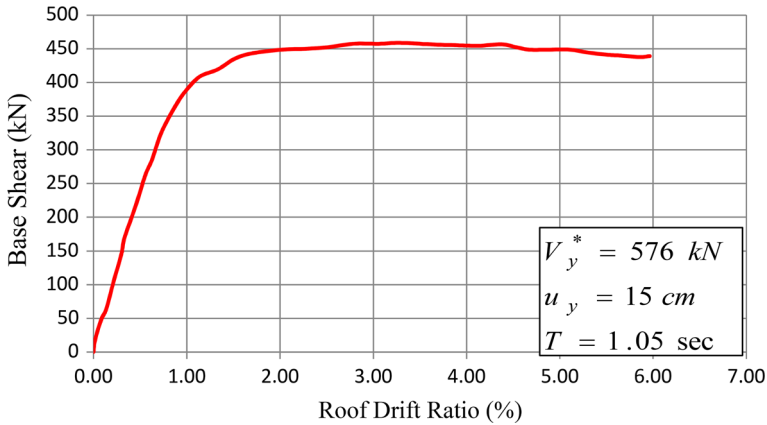


Fig. 13 The capacity/pushover curve of the reference frame

where m^* is the effective modal mass that is equal to $\phi^T M \phi$, ϕ is the normalized modal shape vector, M is the mass matrix, k^* is the effective modal stiffness, and w is the circular frequency of the system. The dynamic properties of the equivalent single-degree-of-freedom (SDOF) system of the reference frame are shown in Fig. 13.

ASCE-7-10 (2010) proposed the following equation for the seismic-based shear, V , of mid-rise buildings (with periods longer than T_s and shorter than T_L):

$$V = C_s W = \left(\frac{S_{D1}}{T} \right) \cdot W \tag{9}$$

where T_s = short-period transition period; T_L = long-period transition period; C_s = seismic response coefficient; W = the effective seismic weight; SD_1 = the design earthquake spectral response acceleration parameter at 1 s period; R = the response

modification factor; I_e = the importance factor; and T = the fundamental period of the reference frame.

To determine the lumped mass of the studied specimens, the ratio of the capacity base shear of the specimens and equivalent SDOF system should be equal to the ratio of their design seismic base shear. Therefore:

$$\frac{V_{\text{column,capacity}}}{V_{\text{SDOF,capacity}}} = \frac{V_{\text{column,demand}}}{V_{\text{SDOF,demand}}} = \frac{\frac{m_{\text{column}}}{R_{\text{column}} T_{\text{column}}}}{\frac{m_{\text{SDOF}}}{R_{\text{SDOF}} T_{\text{SDOF}}}} \quad (10)$$

Suppose $R = \mu$ and $T = 2\pi\sqrt{m/k}$:

$$\frac{m_{\text{column}}}{m_{\text{SDOF}}} = \frac{k_{\text{column}}}{k_{\text{SDOF}}^*} \left(\frac{\mu_{\text{column}} V_{\text{column,capacity}}}{\mu_{\text{SDOF}} V_{\text{y,SDOF}}^*} \right)^2 \quad (11)$$

where $V_{\text{column,capacity}}$ = the capacity base shear of the studied specimens that can be found from test data shown in Fig. 4; $V_{\text{SDOF,capacity}}$ = the capacity base shear of the equivalent SDOF system that is equal to V_y^* ; $V_{\text{column,demand}}$ = the design base shear of the studied specimens; $V_{\text{SDOF,demand}}$ = the design base shear of the equivalent SDOF system; m_{column} = the effective lumped mass of the mathematical model of the studied specimens (located at the top of column, as shown in Fig. 5); m_{SDOF} = the effective mass of the 1st mode of the reference frame; μ_{SDOF} = the displacement ductility capacity of the equivalent SDOF system; μ_{column} = the displacement ductility of the studied specimens that can be found from the test data shown in Fig. 4; k_{SDOF}^* = the effective stiffness of the 1st mode of the reference frame; and k_{column} = the effective stiffness of the studied specimens that can be found from the test data shown in Fig. 4.

4.2 Ground motions

Twenty-two far field ground motions recommended by FEMAP695 (2009) were used as both mainshock and aftershock records. To ensure broad representation of different recorded earthquakes, sets of ground motions contain records selected from all large-magnitude events in the PEER NGA database (PEER 2006). The ground motion intensity was measured using elastic spectral acceleration, S_a , at the fundamental period of the structure. Because the period of the specimen was different from the period of the reference frame, the time scale of the candidate motions was condensed by the ratio of their periods.

5 Results and discussion

In determining the capacity curve for the pre-event building, FEMA-306 proposed modified concrete and masonry wall properties to reflect the results of damage investigations, as shown in Fig. 14. In this guideline, the effects of damage on component behavior were modeled using three modification factors: effective initial stiffness (I_k), expected strength (I_Q) and deformation acceptability limits (I_D). The values of the modification factors depend on the behavior mode and the severity of the damage to the individual component. The factors were inferred from individual cyclic–static tests by examining the change in the force–displacement response from cycle to cycle as the displacements were increased.

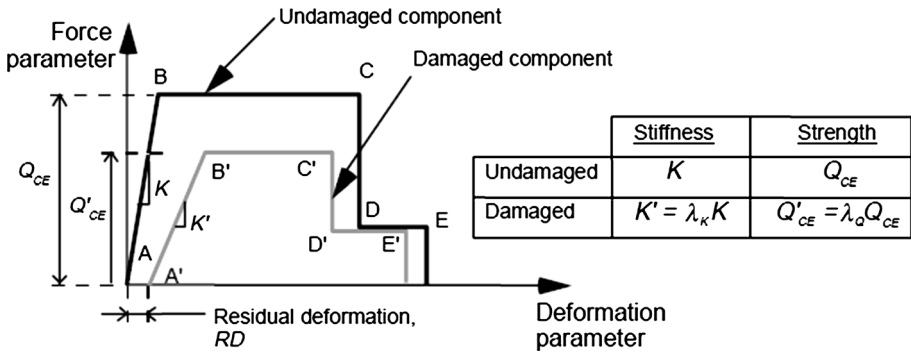


Fig. 14 Damaged and undamaged component modeling criteria (FEMA-306 1999)

The initial cycles were considered representative of the damaging earthquake, and the subsequent cycles representative of the behavior of an initially damaged component.

The effects of the characteristics of input ground motions were not included in the methodology of FEMA-306 to calculate the modification factors. Moreover, in this guideline, the maximum crack width defines the damage severity. Using the qualitative descriptions of damage states from the guideline results in varying tagging decisions depending on the inspection personnel. Following this, the authors propose similar modification factors for RC columns using residual displacement as a damage indicator and probability approach with the use of IDA.

To determine the strength deterioration of the studied columns, the fragility surfaces of intact and mainshock-damaged columns were calculated using the illustrated method in Sect. 3. The collapse fragility of undamaged columns was computed using Eq. 4, as shown with the continuous line in Fig. 15. The median and the logarithmic standard deviations of the collapse capacity of the undamaged column are 1.21 g and 0.45, respectively.

The collapse fragility surfaces (with respect to aftershocks) for the mainshock damaged column are developed here for two levels of damage using the presented methodology in Sect. 3: (1) concrete spalling and (2) concrete crushing. For simplicity, the traces of the fragility surface in the planes of the residual displacements have been shown in Fig. 15 by a dashed line. Unlike the mainshock response, the aftershock responses are sensitive to different polarities. Therefore, both aftershock responses were computed by applying positive and negative factors to the aftershock records, and the smallest aftershock spectral acceleration that induced collapse was used to calculate the fragility function.

Figure 15 shows that the dependence of residual capacity on the residual drift ratio is more for concrete spalling than for concrete crushing. Using the mean values of the fragility curves ($S_{a,50\%}$), as shown in Fig. 15, to represent the strength capacity of the columns, the strength modification factors for damaged columns can be found from Eq. 12. The residual capacity of a column with concrete spalling can be decreased by approximately 9–22 % based on the residual drift ratio. The decrease will be raised to 25–35 % when the column experiences concrete crushing during a mainshock.

$$\lambda_Q = \frac{(S_{a,50\%})_{\text{Damaged column}}}{(S_{a,50\%})_{\text{Intact column}}} \tag{12}$$

To estimate the stiffness modification factor, the change in the fundamental period of the studied columns after mainshock is assumed to be a random variable. The change in the

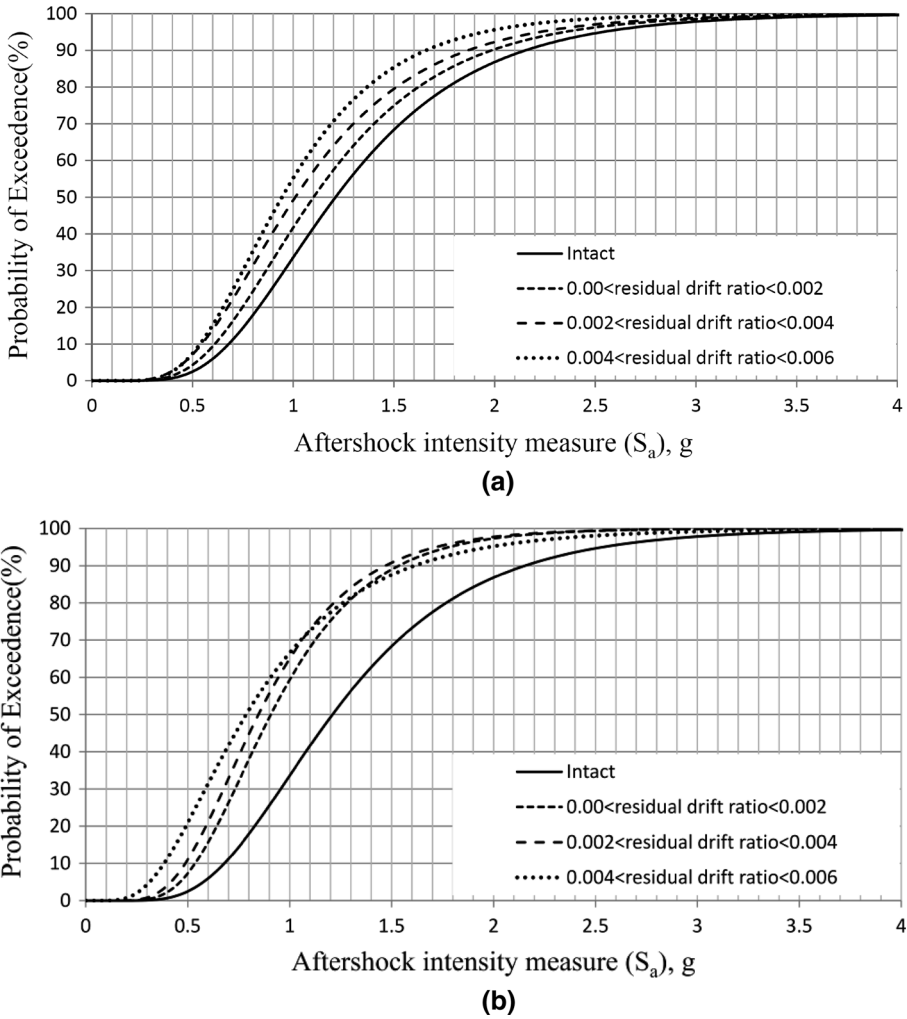


Fig. 15 The collapse fragilities of a damaged column: **a** concrete spalling due to mainshock, **b** concrete crushing due to mainshock

fundamental period of the specimens follows a lognormal distribution, and the median value of this distribution was considered to be the stiffness modification factor.

Figure 16a shows that the values of the stiffness modification factors depend on the severity of the damage because the amount of residual displacement is not an impressive factor, i.e., the change in the effective initial stiffness is a function of the maximum displacement. Because the strength modification factors depend on the severity of the damage and the permanent displacement (Fig. 16b), not only could the maximum displacement affect the residual strength of damaged columns, but the history of response is another effective parameter.

Ludovico et al. (2012) proposed the experimental-based calibration of modification factors for plastic hinges of damaged columns representative of existing buildings with

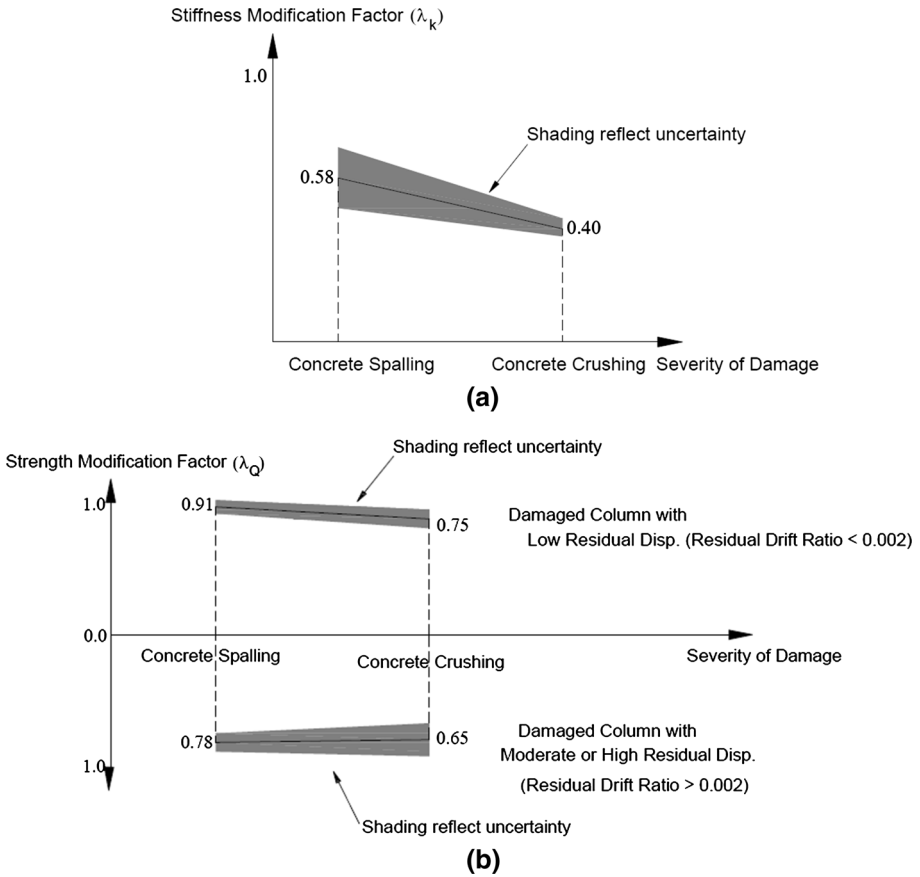


Fig. 16 Column modification factor and damage severity. **a** Stiffness modification factor, **b** strength modification factor

design characteristics nonconforming to present-day seismic provisions. They gathered the modification factors from 18 cyclic tests by examining the change in the force–displacement response from cycle to cycle. To this end, initial cycles were considered representative of the behavior of intact elements, whereas subsequent cycles were for the damaged component. Following this, Ludovico et al. (2012) proposed stiffness and strength modification factors as below:

$$\lambda_k = 1 - \left(1.10 - 1.16 \times \left(\frac{\theta}{\theta_y} \right)^{-0.87} \right) \tag{13}$$

$$\lambda_Q = 1 - 0.07 \times \left(\frac{\theta}{\theta_y} - 1.0 \right)$$

where θ/θ_y is the ductility level attained by the column after the damage.

Using the above equations and the values from Table 2, the modification factors for the studied specimens are calculated, as listed in Table 3.

Table 3 Modification factors for the studied specimens using the proposed formulas of Ludovico et al. (2012)

Experienced damage state during mainshock	λ_k	λ_Q
Concrete spalling	0.4	0.9
Concrete crushing	0.2	0.7

A comparison of the listed values in Table 3 and Fig. 16 reveals that using cyclic tests to estimate the strength modification factor gives acceptable results. However, there is a meaningful difference between the evaluated stiffness modification factors. The authors believe that using nonlinear dynamic analysis instead of cyclic tests is the main source of this disagreement, meaning that the earthquake loading cycle after experiencing maximum displacement by the specimens resurrected them. Therefore, using cyclic tests underestimates the stiffness modification factors.

6 Summary

The purpose of this study is to provide practical criteria for evaluating earthquake damage to RC columns. The procedures in this paper are intended to characterize the observed damage caused by the earthquake in terms of the loss in the column's performance capability. To eliminate various tagging decisions dependent on inspection personnel, the residual displacement and visual damage indicator are jointly considered here to estimate the damage severity. A probabilistic method is proposed to calculate the fragility surfaces of the strength and stiffness deterioration of damaged columns.

A strong column database is available, but the definitions of different damage states are dependent on the observer. Following this, five RC columns, which were tested by the third author, were considered to develop the fragility surface using the proposed methodology.

To perform mainshock–aftershock analysis, the mainshock ground motions from FEMAP695 was used as the aftershock records. Although, the aftershock ground motions have dissimilar characteristics as the mainshock ground motion, authors believe that using 22 records for aftershock could overcome to this limitation.

The results show that experiencing slight damage, e.g., concrete spalling, during mainshock by a column decreased its residual capacity by approximately 9–22 %, based on the amount of permanent displacement, while severe damage, e.g., concrete crushing, raised this range to 25–35 %. The stiffness deterioration is only dependent on the severity of damage, and the amount of residual displacement is not an impressive factor. Moreover, damage causes a more severe deterioration of stiffness than strength, so that slight and severe damage degraded the stiffness by approximately 42 and 60 %, respectively.

Comparing the results of this study to the proposed values by Ludovico et al. (2012) shows that using cyclic tests overestimates the stiffness modification factors but gives acceptable results for the strength modification factors.

All of the studied columns have a quite high axial force (between 0.16 and 0.31 $A_g f'_c$) with flexure-critical mode, which is common in reinforced concrete moment frames. The results may be changed in other cases.

To derive more reliable modification factors, further tests are necessary to enrich the existing database; furthermore, an extension of the procedure on RC beams and shear-critical RC columns is under investigation.

References

- ATC (1989) ATC-20 procedures for post earthquake safety evaluation of buildings. Applied Technology Council, Redwood City
- ATC (1995) ATC-20-2, addendum to the ATC-20 post earthquake building safety evaluation procedures. Applied Technology Council, Redwood City
- ATC (1999) FEMA306: evaluation of earthquake damaged concrete and masonry wall buildings: basic procedures manual (ATC-43 project). Applied Technology Council, Redwood City
- Bazzurro P, Cornell CA, Menun CA, Motahari M, Luco N (2006) Advanced seismic assessment guidelines, PEER 2006/05. Pacific Earthquake Engineering Research Center, University of California, Berkeley
- Chang G, Mander J (1994) Seismic energy-based fatigue damage analysis of bridge columns: part I—evaluation of seismic capacity, NCEER-94-0006. State University of New York at Buffalo, Department of Civil and Environmental Engineering, New York
- Christopoulos C, Pampanin S, Priestley MJ (2003) Performance-based seismic response of frame structures including residual deformations. Part I: single degree of freedom systems. *J Earthq Eng* 7(1):97–118
- Clough RW, Penzien J (1993) Dynamic of structures, 2nd edn. McGraw-Hill, New York
- Elwood K, Moehle J (2003) Shake table tests and analytical studies on the gravity load collapse of reinforced concrete frames, PEER 2003/01. Pacific Earthquake Engineering Research Center, University of California, Berkeley
- FEMA (2009) Quantification of building seismic performance factors, FEMA P695. Applied Technology Council for the Federal Emergency Management Agency, Washington
- JBDPA (2001) Guidelines for post-earthquake damage evaluation and rehabilitation. Japan Building Disaster Prevention Association, Tokyo (**in Japanese**)
- Khanmohammadi M (2006) Displacement and damage index criteria in performance-based seismic design of RC buildings. School of Engineering, University of Tehran, Tehran
- Lee W, Billington S (2010) Modeling residual displacements of concrete bridge columns under earthquake loads using fiber elements. *J Bridge Eng* 15(3):240–249
- Luco N, Bazzurro P, Cornell CA (2004) Dynamic versus static computation of the residual capacity of a mainshock-damaged building to withstand an aftershock. In: 13th world conference on earthquake engineering, Vancouver
- Ludovico MD, Polese M, Gaetani d'Aragona M, Prota M (2012) Plastic hinges modification factors for damaged RC. In: 15WCEE, Lisbon
- Marefat MS, Khanmohammadi M, Baharani MK, Goli A (2006) Experimental assessment of reinforced concrete columns with deficient seismic details under cyclic load. *Adv Struct Eng* 9(2):337–347
- Moshref A, Tehranizadeh M, Khanmohammadi M (2014) Investigation of the reliability of nonlinear modeling approaches to capture the residual displacements of RC columns under seismic loading. *Bull Earthq Eng* 13(8):2327–2345
- Opensees Development Team (2002) Open system for earthquake engineering simulation. Opensees Development Team, Berkeley
- Pampanin S, Christopoulos C, Priestley MJN (2003) Performance-based seismic response of frame structures including residual deformations. Part II: multidegree of freedom systems. *J Earthq Eng* 7(1):119–147
- Paulay T, Priestley MJN (1992) Seismic design of reinforced concrete and masonry buildings. Wiley, New York
- PEER (2006) PEER NGA database. Retrieved from Pacific Earthquake Engineering Research Center, University of California, Berkeley. <http://peer.berkeley.edu/nga/>
- Ryu H, Luco N, Uma S, Liel AB (2011) Developing fragilities for mainshock-damaged structures through incremental dynamic analysis. In: 9PCEE, vol 225. Building an Earthquake-Resilient Society, Auckland, pp 1–8
- Shin YB (2007) Dynamic response of ductile and non-ductile reinforced concrete columns. University of California, Berkeley
- Smyrou E, Tasiopoulou P, Bal İ, Gazetas G, Vintzileou E (2011) Structural and geotechnical aspects of the Christchurch (2011) and Darfield (2010) earthquakes in New Zealand. In: Seventh national conference on earthquake engineering, Istanbul, Turkey
- Stanton J, McNiven H (1979) The development of a mathematical model to predict the flexural response of reinforced concrete beams to cyclic loads, using system identification, EERC 79-02. Pacific Earthquake Engineering Research Center, Berkeley
- USGS (2011) United States Geological Survey. Retrieved from <http://www.usgs.gov/>
- Yazgun U (2009) The use of post-earthquake residual displacements as a performance indicator in seismic assessment. ETH Zurich University, Zurich